EPJ manuscript No.
(will be inserted by the editor)

About electrons in Triplet Production

M. L. Iparraguirre and G. O. Depaola

Facultad de Matemática, Astronomía y Física, Universidad Nacional de Córdoba. Dr. Medina Allende s/n. Ciudad Universitaria. Córdoba 5008. Argentina., e-mail: ipa@famaf.unc.edu.ar, e-mail: depaola@famaf.unc.edu.ar

June 12, 2014

Abstract. It is usually assumed that the difficulties arising from the indistinguishability of the two electrons in the triplet produced by photons of high energy in the field of an electron may be avoided simply by ruling out the contributions of all the Feynmann diagrams as well as the Borsellino. In this way, the question of indistinguishability becomes meaningless, there is a clear distinction between the recoil electron and the pair electron; and it is well-known that the entire mechanism works well if the photon energy is high enough. In this work we have analyzed the eight Feynmann diagrams and we have shown that for energies lower to $\sim 1000mc^2$, the assumption just described is not a good approximation. We propose a different way to work: we classify the electrons into the less energetic and the most energetic ones without taking into account their origin, and to define, only to keep the experimental treatment that the less energetic ones will be called the recoil electrons, while the most energetic ones will be called the pair or created electron. Under these conditions (lower or higher energy value), we have calculated the contribution of the different diagrams to the distribution, and how these distributions are modified by introducing a threshold for the momentum detection for electrons.

arXiv:1406.3001v1 [hep-ph] 11 Jun 2014

1 Introduction

When a high energy gamma-ray interacts with the electric field of an electron, it could be annihilated in a pair e^- e^+. The original e^- can absorb enough momentum to be detected; so, in the final state, one can observe the particles of the created pair and the recoil electron, constituting a so called triplet.

Correspondence to: depaola@famaf.unc.edu.ar

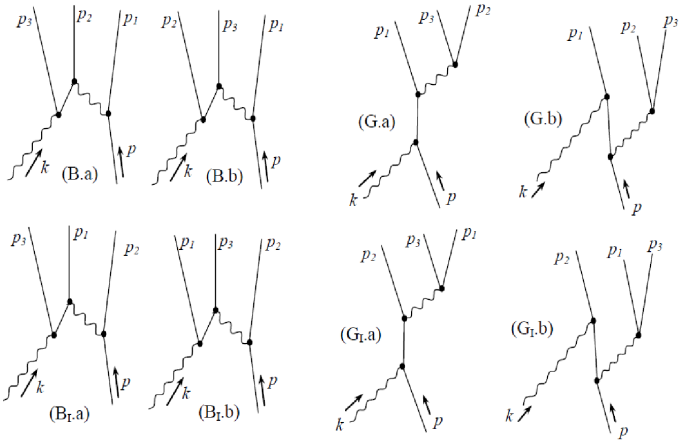

Fig. 1. Feynman diagrams describing photoproduction of e^+ e^- pairs on free electrons.

Due to the indistinguishability of the electrons, it is not possible to know who the created electron is and who the recoil electron is. It is usual to label the lower energy electron as the recoil electron because it is the most probable case for high energy gamma-rays..

The moment (or energy) distributions for the three particles can be calculated by using the standard technique of the quantum electrodynamics in the lower approximation order. For this process:

$$\gamma + e^- = e^+ + e^- + e^-.$$

one has 8 Feynman diagrams, two of then, called the Borsellino diagrams [1] (Ba and Bb in 1), made the main contribution to the total cross section of the process ([2], [3] [4]). Many authors put focus only in these diagrams to obtain the momentum or angular distributions of the particle (Boldyshev et. al. [5] made an extensive calculation, for example).

The use of only these two diagrams simplifies the interpretation of the roll of the electrons since, according to figure 1, it is clear that p_1 distribution corresponds to the recoil electron and p_2 to the created electron. This is a good approximation for high energy limits that we have established in this work as $\omega \geq 1000mc^2$. This facility is lost when we include the exchange diagrams.

In this work we have shown that for medium and lower energies, the contribution of the other diagrams, in particular the inclusion of the exchange of the Borsellino diagrams overestimate the total cross section making it necessary to take into account all the diagrams. Also, the

probability that the created electron could acquire energy lower than the recoil electron can be significant in the medium and lower regime, and the inclusion of the exchange diagrams change the roll of these particles. This is important since in an experiment it is not possible to distinguish between the pair electron and the recoil electron. Our proposal is to calculate the energy distribution in a situation more similar to the experimental setup, that is, to calculate the energy distribution of the lower energetic electron and the energy distribution of the higher energetic electron without taking into account the origin of the electrons.

In section 2, we have given a brief discussion about how we have calculated the cross section from the Feynman diagrams, which variables we have chosen to integrate analytically and which ones, in numerical form, and how to find the limits that the cinematic has imposed on the variables of interest. The most important diagrams are the Borsellino one and the respective exchange where the labels of the electrons are inverted. We concentrate on the calculations based on these diagrams.

The section 3 shows the energy distribution given by the different terms of the scattering matrix. Also, we have shown their overlapping. We have also tried to show where only the use of the Borsellino diagrams is a good approximation analyzing this overlapping of the distribution that quantifies, in some sense, the probability the roll is exchanged between the electrons. In section 3a, we have calculated the energy distribution obtained for the lower energetic electron and for the higher energetic electron in 3b. We have also shown the contribution for many terms of the scattering matrix.

2 Feynman diagrams and some kinematics considerations

The 4-momentum conservation for this collision is written as:

$$k + p = p_r^- + p^- + p^+ = p_1 + p_2 + p_3.$$

As usual, in this work we take $\hbar$ and c equal to 1, and then, in the laboratory system, $k = (\omega, \omega\hat{k})$, and $p = (m,\mathbf{0})$, where $\hat{k}$ is the unit vector of the incidence γ - ray direction. We call p_1 and p_2 to the 4-momentum of the electrons that, depending on the diagrams, (figure 1) can be the recoil electron or the momentum of the created electron or conversely. p_3 is the 4- momentum of the positron.

The cross section of this process can be calculated by using the standard technique. The 8 Feynman diagrams are shown in figure 1, 2 of them, the $B.a$, $B.b$ are the Borsellino diagrams, the other 2, $G.a$ and $G.b$, are called $\gamma - e^-$ and the other 4 ($B_I.a$, $B_I.b$, $G_I.a$, $G_I.b$) are the exchange diagrams due to the indistinguishability between the recoil electron and the electron created (in this last 4th case, the roll of p_1 and p_2 interchanges).

Looking at the G diagrams, one can see that these are basically Compton diagrams, with a created pair at the end of the virtual photon, so it is expected that the contributions to the cross section of these diagrams will decrease with the gamma-ray energy.

To exemplify the calculation, we have neglected the G diagrams (however, in our final results we have included all of them). Under these conditions, the matrix elements to be calculated are:

$$\begin{aligned} |M|^2 &= |M_B - M_{BI}|^2 \\ &= |M_B|^2 + |M_{BI}|^2 - |M_B M_{BI}^* - M_B^* M_{BI}| \end{aligned} \tag{1}$$

The first effect to notice with respect to the usual calculations using only the Borsellino diagrams, is the introduction of the term $|M_{BI}|^2$ which consists in the exchange of the label between the two electrons, that is $|M_B(1,2)|^2 + |M_{BI}(2,1)|^2$.

The second and the most important contribution is the interference term which give how much overlapping is, in the phase space, between the variables; for example, once it integrates over all the variables, except for p_1

$$\frac{d\sigma}{d^3\mathrm{p}_1} = \iiint |M|^2 \cdots d^3\mathrm{p}_2 \mathrm{d}^3\mathrm{p}_3$$

noindent one will have the probability density that the recoil electron and the created electron, and it can take the value p_1.

The inclusion of the exchange term has made it necessary to multiply the cross section by the 1/2 factor to avoid double-counting due to the indistinguishability of the electrons.

The triple differential cross section for the process is:

$$d\sigma = \frac{\alpha r_0^2}{4\pi^2}\frac{1}{\omega m}\frac{d^3\overrightarrow{\mathrm{p}_1}}{E_1}\frac{d^3\overrightarrow{\mathrm{p}_2}}{E_2}\frac{d^3\overrightarrow{\mathrm{p}_3}}{E_3}\delta^4\left(\sum p_f - \sum p_i\right)\left(\frac{4m^6}{e^6}|M|^2\right) \tag{2}$$

Since in this work we are interested to describe the electrons distributions, we have used the delta function to integrate over the positron variables ($\overrightarrow{\mathrm{p}_3}$),

$$\begin{aligned} d\sigma =& \frac{\alpha r_0^2}{2\pi}\frac{1}{\omega m}\frac{d^3\overrightarrow{\mathrm{p}_1}}{E_1}\frac{d^3\overrightarrow{\mathrm{p}_2}}{E_2}\frac{1}{E_3(\overrightarrow{\mathrm{p}_1},\overrightarrow{\mathrm{p}_2})} \\ & \delta\left(\sum E_f - \sum E_i\right)\left(\frac{4m^6}{e^6}|M|^2\right) \end{aligned} \tag{3}$$

where in the M we also must substitute E_3 and $\overrightarrow{\mathrm{p}_3}$ by the expressions in function of $\overrightarrow{\mathrm{p}_1}$ and $\overrightarrow{\mathrm{p}_2}$ using the conservation law.

The last delta function has been chosen to integrate over the azimuthal angle of electron labeled 2 φ_2:

$$\begin{aligned} d\sigma =& \frac{\alpha r_0^2}{2\pi}\frac{1}{\omega m}\frac{d^3\overrightarrow{\mathrm{p}_1}}{E_1}\frac{\mathrm{p}_2^2 \sin\theta_2 \mathrm{dp}_2 \mathrm{d}\theta_2}{E_2} \\ & \frac{1}{2\pi \mathrm{p}_1 \mathrm{p}_2 \sin\theta_1 \sin\theta_2 |\sin(\varphi_2 - \varphi 1)|}\left(\frac{4m^6}{e^6}|M|^2\right) \end{aligned} \tag{4}$$

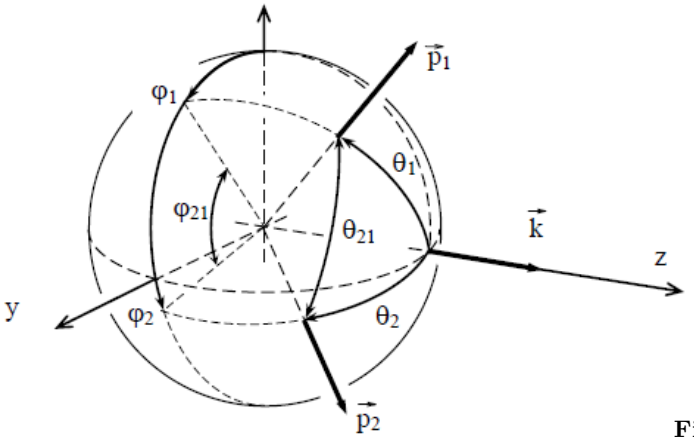

Fig. 2. Angles after integate over positron varables

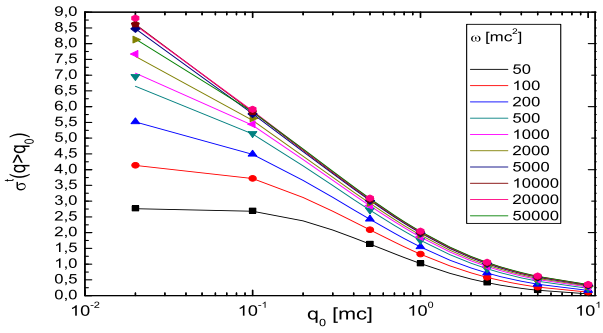

Fig. 3. Comparison of total cross section in function of threshold momentum for many gamma rays energies (lower energy at bottom) between our calculation (line) and table V in [5] (symbols)

The absolute value of the expression corresponds to, once φ_1 is fixed, two possible values to φ_2 that are given by the same θ_{21} (see figure 2). The φ_2 value must void the following expression (where x represents the other variables):

$$g(x,\varphi_2) = \omega + m - E_1 - E_2 - E_3(\vec{p_1},\vec{p_2}) \qquad (5)$$

The condition $g(x,\varphi_2)=0$ gives the following expression for the $\cos\varphi_{21}$ where $\varphi_{21}=|\varphi_2-\varphi_1|$:

$$\cos\varphi_{21} = \frac{1}{p_1 p_2 \sin\theta_1 \sin\theta_2}\left[(\omega+m)(m-E_1-E_2)+ E_1E_2+\omega(p_1\cos\theta_1+p_2\cos\theta_2)-p_1p_2\cos\theta_1\cos\theta_2\right] \qquad (6)$$

this expression is not necessarily < 1 when $\vec{p_1}$ and $\vec{p_2}$ are into their validity range given by the kinematics (see figure 3 in ref [6]). Once fixed $\vec{p_1}$, this expression is very restrictive to $\vec{p_2}$. Defining F as:

$$F = -p_2^2\cos^2\theta_2 G + 2p_1\cos\theta_2(\omega-p_1\cos\theta_1)C + p_1^2p_2^2\sin^2\theta_1 - C^2 \qquad (7)$$

where:

$$C = (\omega+m)(E_1+E_2-m)E_1E_2-\omega p_1\cos\theta_1)$$

$$G = \omega^2 + p_2^2 - 2\omega p_1\cos\theta_1)$$

the differential cross section can be written as:

$$d\sigma = \frac{\alpha r_0^2}{2\pi}\frac{1}{\omega m}\frac{d^3\vec{p_1}}{E_1}\frac{p_2^2\sin\theta_2 dp_2 d\theta_2}{E_2}\frac{1}{\pi\sqrt{F}}\left(\frac{4m^6}{e^6}|M|^2\right) \qquad (8)$$

where the extreme values of θ_2 (once $\vec{p_1}$ and p_2 are into their validity range) must satisfy the condition $F \geqslant 0$

$$\cos\theta_2^{\pm} = \frac{(\omega - p_1\cos\theta_1)C \pm p_1\sin\theta_1\sqrt{p_2^2G-C^2}}{p_2 G} \qquad (9)$$

(it has been found that the extreme values for θ_2 are very close each other).

The differential cross section (eq. 8) admits two analytical integrations, one trivial over φ_1 since in any stage of the calculation one can write the cross section as $d\sigma = d\sigma^t - d\sigma^l\cos 2\phi_1$, the other chosen variable was θ_2 (we have omitted the final expression because it is too long), so finally we have an exact expression for the differential cross section according to $d\sigma = d\sigma(p_1,p_2,\theta_1)$. To obtain the momentum distribution we must continue with numerical integrations.

In order to test our calculation, in figure 3 we compare the total cross section in function of the threshold momentum (only for the recoil electron) obtained in this work (lines) with the table V in [5] (symbols) obtained using only the Borsellino diagram in both cases. One can see that for $\omega \geq 5000mc^2$ the curves can not distinguish the asymptotic expression [6] when $q_0 \geq 0.1m$. Bernard [7] also produces these curves including all the terms (figure 6 in [7]) but it is noticed that the values obtained are lower respect to Boldyshev and this work, probably because all the terms have been used (and in this case it is not clear how the threshold is applied).

3 Energy distribution for the electrons

To obtain the energy distribution of p_1 that, as one can see from the Feynman diagrams in fig.1, which represents the recoil electron in $|M_B|^2$ and the created electron in $|M_{BI}|^2$, we have integrated (in numerical form) over $0 \leq \theta_1 \leq \theta_{1max} = \arccos\left(\frac{\omega(E_1-m)+m(E_1+m)}{\omega p_1}\right)$ (the maximum θ allowed by the kinematics, eq. 28 in [5]) and over $p_{2\min}(\theta_1,E_1) \leq p_2 \leq p_{2\max}(\theta_1,E_1)$ (eq.7.5 in [4]), roots of $p_2^2G = C^2$ (see figure 3 in [6]). Another fact to take into account is that

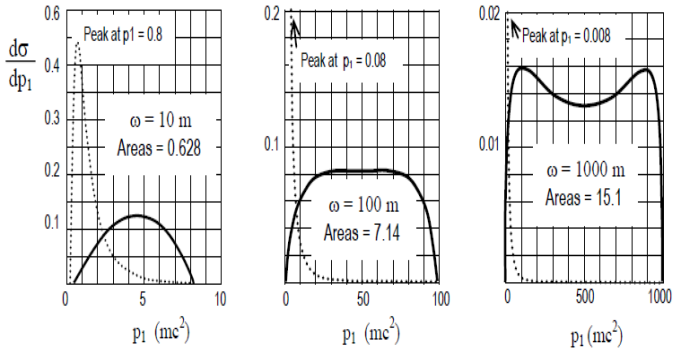

Fig. 4. Energy distribution for p_1 obtained using only $|M_B|^2$ where represent the recoil electron and the energy distribution obtained using $|M_{BI}|^2$ only, where p_1 is the electron created in this diagrams.

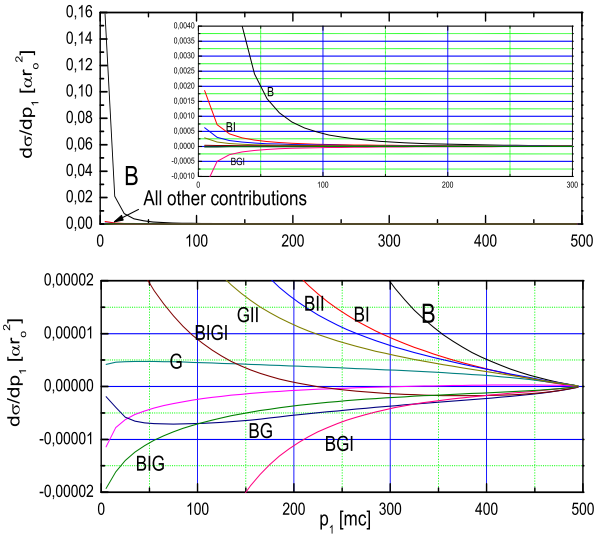

Fig. 5. Energy distribution for the lower energetic electron using different contribution of the Feyman diagram for $\omega = 1000m$.

in an experiment there is a threshold for the momentum detection below where the particle is not detected. In our calculations, we have designated to this limit as q_0 and if $p_{min} \leq q_0$ the integration is done between q_0 and p_{max}.

In figure 4 we show the energy distribution for p_1 obtained using only $|M_B|^2$ where it represents the recoil electron and the energy distribution obtained using $|M_{BI}|^2$, where p_1 is the distribution for the electron created in this case. We show the results for 3 ω different $10m$, $100m$ and $1000m$. As it was mentioned before, the two curves have the same area (shown in the figure and in agreement with that one obtained by Joseph and Rohrlich [2]), the $|M_B|^2$ was trunk to see $|M_{BI}|^2$. The peak of the $|M_B|^2$ is found when $p_1 \backsimeq 8/\omega$. If the value for the threshold detection for p_1 is around $1m$, in general, only one sees a decreasing distribution for the electron recoil.

From this figure, one can deduce that for $\omega \lesssim 1000m$ the probability that the recoil electron has acquired energy greater than the created electron, is not so small, so to compare the theoretical distribution with the experimental data we propose to calculate $d\sigma_T(p_1 < p_2)/dp_1$ and $d\sigma_T(p_1 > p_2)/dp_1$ ($d\sigma_T$ is the sum of all terms) obtaining in this way the energy distribution for the lower and higher energetic electron whatever their origin is.

3.1 Energy distribution for the lower energetic electron

In the figure 5 we show, for $\omega = 1000m$, the energy distribution for the lower energetic electron using different contribution of the Feyman diagrams. The symbology used is the following one: B represents the contribution of $|M_B|^2$, BII for $|M_{BI}|^2$, $BI \equiv |M_{BI}M^*_{BI} - M^*_{BI}M_{BI}|^2$, $G \equiv |M_{\gamma e}|^2$ and so on. Figure 4a shows the full scale and one can see how dominant is the $|M_B|^2$ contribution. The figure 4b is the same as figure 4a but with a zoom to see the other contributions. In table 1 we compare the contribution of each term in relation to the areas of each curve respect to the area of the Borsellino term (in percentage) for three gamma-ray energies. It is noteworthy that the only inclusion of the Borsellino exchange diagram imply a correction of 8.15 % for $100m$ and this overestimates the correction that includes all terms, which is 5.88 %.

A better idea about the relation between the Borsellino diagrams and the other terms can be carried out by showing the relation $(d\sigma_B/dp_1)/(d\sigma_X/dp_1)$ (where X represents any of the other terms). The results are shown in figure 6 for three different ω and an enlargement in the p_1 scale for $\omega = 1000m$. In this graph, it is possible to see that for lower value of p_1 the curves are seen as a linear function of p_1 (see 6d). Another interesting behavior that one can see is that the axes change very little whereas the abscissa is multiplied by 100, this indicates that the slope in the linear part is proportional to ω^{-1}

Taking into account that the interval of p_1 where the probability is not so small, and does not extend to where ω increases; the zone where the slope is proportional to ω^{-1} does not depend on ω

In this way, the total correction for energy distribution obtained through the Borsellino terms can be written as, with an accuracy of 1%, $d\sigma_{tot}/dp_1 = d\sigma_B/dp_1$ when $p_1 \leq$ m and for $m \leq p_1 \leq 10$m, so we propose:

$$\frac{d\sigma_{tot}/dp_1}{d\sigma_B/dp_1} = \frac{2.36}{\omega}(p_1 - m) \qquad (10)$$

In conclusion, the energy distribution for the lower energetic electron can be expressed as ($m \leq p_1 \leq 10$m):

$$\frac{d\sigma_{tot}}{dp_1} = \frac{d\sigma_B}{dp_1}\left(1 + \frac{2.36}{\omega}(p_1 - m)\right) \qquad (11)$$

The next step is to find a handle expression for $d\sigma_B/dp_1$, in this sense one can find in [5] an analytical expression for $d\sigma_{Boldyshev}/dXd\Delta^2$ (eq. 37) where $X = 2m(E_1 - m)$. In the same work, eq. 47 give the integration of eq. 37

$\omega[m]$	$B[\alpha r_0^2]$	BII/B	BI/B	G/B	GII/B	GI/B	BG/B	$BIGI/B$	BGI/B	BIG/B	$Total$
100	2.22	3.20	4.95	0.40	1.71	-0.34	-0.48	-0.46	-3.4	-0.62	5.88
1000	3.19	0.67	1.46	0.05	0.36	-0.021	-0.07	0.07	-1.0	-0.07	1.45
10000	3.46	0.11	0.30	0.0057	0.065	-0.0016	-0.0076	0.0077	-0.22	-0.008	0.25

Table 1. Contribution of the matrix terms respect to the Borsellino term (in percent) for three gamma ray energies

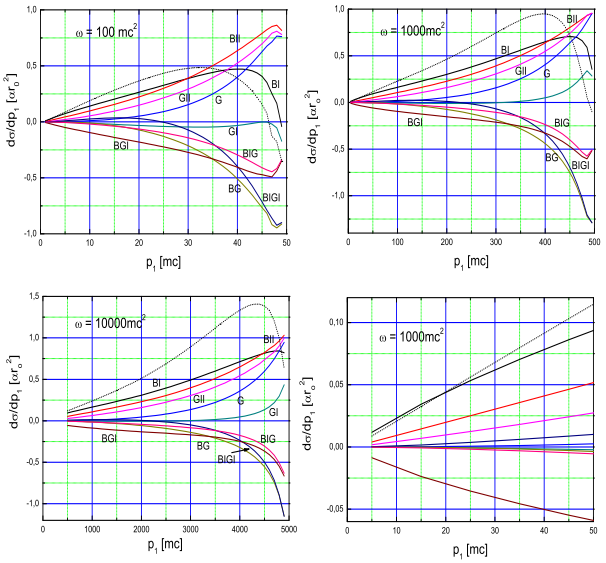

Fig. 6. Relation between the Borsellino diagrams and the other terms. The dot line is the sum of all contribution.

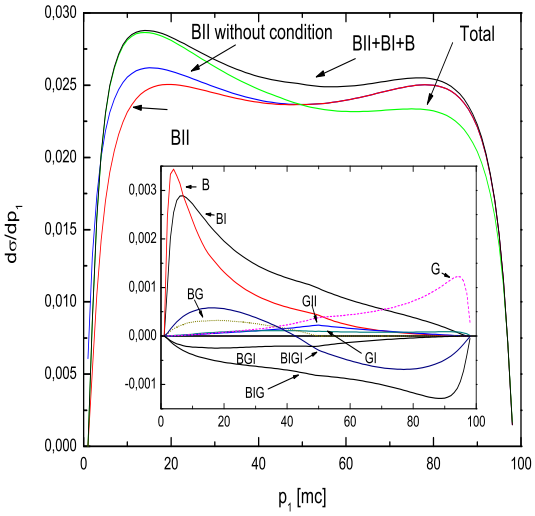

Fig. 7. More energetic electron energy distribution, contribution from different terms.

over Δ^2 and, with a simple change of variables, can be written in terms of p_1. The eq. 47 is not very short and it includes the Euler's logarithm but more handled that our numerical integration.

3.2 Energy distribution for the more energetic electron

Now we present the results of the integration over p_2 with the condition that it should be greater than a threshold detection q_0 and lower than p_1. In figure 7 we compare the obtained distribution taking into account different terms of the matrix for $\omega = 100m$ and $q_0 = 1mc$. In this graph, one can see that the exchange Borsellino diagrams is dominant and give a curve very symmetric similar to the nuclear case (it can be shown that the BII is similar to the Bethe-Heitler distribution and that for $\omega = 10000mc^2$ it can be indistinguishable between them. In the same figure, we show the curve obtained for the same term without any condition over the momentum; in this case the apparent symmetry is lost and one has more probability in the range lower than $\omega/2$. We also show the other terms, the total (sum of all the terms, which represents that one measure in an experiment taken as the most energetic electron like the created electron) and the sum of $BII + BI + B$. One can see that $BII + BI + B$ are the principal contribution but it overestimates the total distribution after the first peak. For $\omega = 1000mc^2$ the difference between this partial sum and the total is 1.5% approximately (it contains more than the 90% of the case). In this case, the main term is BII and one can repeat the same table 1 but, as it is expected, one can obtain the same values by making the following exchange in the notation $B \leftrightarrow BII$, $G \leftrightarrow GII$, $BG \leftrightarrow BIGI$ and $BIG \leftrightarrow BGI$

To analyze the effect of the threshold detection, we have used the BII term in a extreme case, $q_0 = 10mc$, as an example since in this term, p_1 is the created electron and p_2 is the recoil electron, and this situation has been assumed in the literature. In figure 8 we compare the momentum distribution obtained for $\omega = 100m$ with the only condition that $p_2 \geq q_0$ (solid line), the condition $p_2 \geq q_0$ and $p_2 < p_1$ (more energetic electron, dot line) and $p_2 \geq q_0$ with $p_2 > p_1$ (lower energetic electron, dash line). The area of the first one is $0.109mb$ in agreement with the value obtained by Boldyshev et al (table V in [5]).

Since in the solid curve we only put the threshold on p_2, one can see that the p_1 distribution has the same form than any threshold (figure 5) in the lower range of p_1 and decreases smoothly until $\geq \omega - q_0$ where it becomes zero ($p_1 \geq \omega - q_0 \Rightarrow p_2 < q_0$).

For the most energetic electron (dot curve) one can see that in the first part it is zero until $p_1 > q_0$ since the condition $p_2 < p_1$ implies we do not have any electron

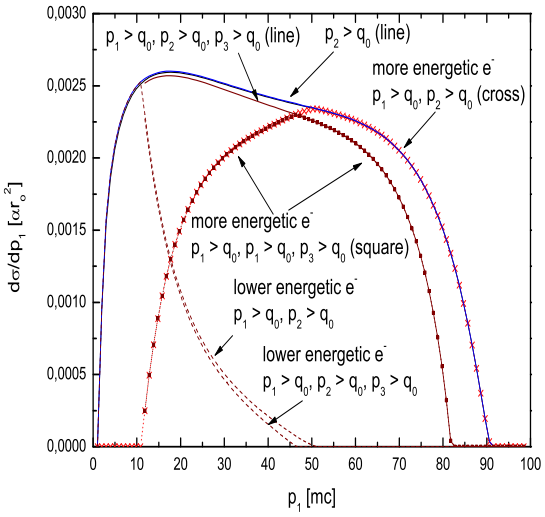
p1 > q0, p2 > q0, p3 > q0 (line)
p2 > q0 (line)
more energetic e-
p1 > q0, p2 > q0 (cross)
more energetic e-
p1 > q0, p1 > q0, p3 > q0 (square)
lower energetic e-
p1 > q0, p2 > q0
lower energetic e-
p1 > q0, p2 > q0, p3 > q0
dσ/dp1 [αr0^2]
p1 [mc]

Fig. 8. Momentum distribution for $\omega = 100m$ and threshold $q_0 = 10mc$ without restriction on the electrons energies (solid line), more energetic electron (dot line) and lower energetic electron (dash line).

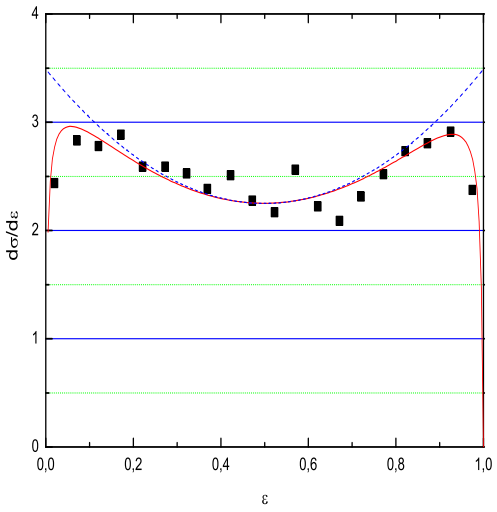

Fig. 9. Comparison between experimantal data [10] and theoretical calculation fot $\omega = 1000m$ and $q_0 = 1mc$.

with $p_1 \leq q_0$. For $p_1 \geq \omega - q_0$ it is also zero due to the same reason: the solid curve.

The lower energetic electrons (dash curve) completed, when is added with the more energetic electron, the total momentum distribution. This distribution, without the condition of a threshold for p_2, show a high peak at $p_1 \simeq 3mc$.

If one put the threshold over p_1 the effect is a cut at $p_1 = q_0$ that is $d\sigma/dp_1 = 0$ for $p_1 < q_0$

The positron distribution is obtained in the same way without any condition over the other electrons energies and not using the exchange terms (B and BII produce the same results and they do so with the other case). Haug shows this distribution (figure 13 in [4]) that is very similar to the distribution shown in figure 7 but it is inverted respect to $\omega/2$, which is unreasonable since it means that the positron, in average, takes more than the half of the energy available.

It is reasonable to think that the threshold detection is for the three particles, in figure 8 we show the momentum distribution for the lower and more energetic electron and the total momentum distribution when the threshold detection if for the three particles. The main change is in the high range of p_1 since the distribution reaches $\omega - 2q_0$ because we now have two particles that necessarily take momentum over q_0. The total cross section for this case is $\sigma(p_1 \geq 10\text{mc}, p_2 \geq 10\text{mc}, p_3 \geq 10\text{mc}) = 0.0533\text{mb}$.

The figure 8 is an extreme case with the objective to make visible the effect of, in a more realistic case, $q_0 << \omega$, and the effect of the threshold can be neglected in the most energetic electrons, and for the lower energetic electron it cuts the events that cannot be detected by modifying only the total cross section, for high gammas-rays energies , the results of $\sigma(q \geq q_=$ in [12] and part of the table 5 in [5] are valid.

In the literature one can find measurements of the energy distribution, for example [8], [9], [10]. Ansoger et al [10] shows the energy distribution in function of $\alpha = (E_+ - E_-)/(E_+ + E_-)$ for 4935 triplet events obtained for gamma-rays energies between $500 - 1000MeV$ and we compare this experimental result with the asymptotic expression obtained by Wheeler and Lamb [11] (for $q_0 = 1mc$) that is very similar to that one obtained by Boldyshev [5]. In figure 9 we reproduce the figure 4 of [10] and we compare it with our distribution obtained for $\omega = 1000m$; to make the comparison, we approximate α parameter of Ansoger as $(E_+ + E_-) = \omega$ so $\varepsilon = (\alpha - 1)/2$.

4 Conclusion

We have calculated the 8 Feynman diagrams to take into account all the terms. From the 9 variables that the process has, we have integrated 6 in analytical form and 2 in numerical way to obtain the momentum distribution of one of the electrons. In the calculation, we have taken into account a threshold for the particle detection.

We have tested our formulas calculating the area of the distribution to obtain the total cross section and we have compared it with the results obtained by Joseph and Rohrlich [2], Mork [3] and Haug [4]. Also, we have obtained a very good agreement with the cross section (using only the Borsellino diagrams) in function of the threshold published by Boldyshev [5] (table V).

Due to the indistinguishability of the electrons, we have obtained the momentum distribution for the lower

and more energetic electron instead of the recoil or created electron according to a real experimental situation.

For each distribution, we have shown the contribution of each term of the scattering matrix and found that de $G(GII)$ and $BIG(BGI)$ has not neglected contribution for $\omega \lesssim 1000m$ (at $\omega = 1000m$ these terms have a contribution of around 1%).

For the lower energetic distribution, we have developed a simple correction of the Borsellino dominant term for this case, B (that can be evaluated more easily using an analytical expression given by Bolsishev [5])

The more energetic distribution (and the distribution for the created electron) show an asymmetry respect to $\omega/2$ (the average energy that the created electron must be $< \omega/2$ since now one have another particles than the electron that must taken energy). As the lower case, $G(GII)$ and $BIG(BGI)$ terms cannot be neglected .

We have shown that the threshold detection for the particles, not only cuts the distributions but also it modifies them, but the modification is not significant when $q_0 << \omega$.

References

1. A. Borsellino, Nuovo Cimento 4, 112 (1947). Rev. Univ. Tuc. 6, 37 (1947)
2. J. Joseph, Y. Rohrlich. Rev. Mod. Phys. 30, 354 (1958).
3. K. J. Mork, Phys. Rev. 160, 1065 (1967).
4. E. Haug, Z. Naturforsch 30a, 1099 (1975).
5. V. F. Boldyshev, E. A. Vinokurov, N. P. Merenkov, and Yu. P. Peresun'ko. Phys. Part. Nucl. 25, 3 (1994).
6. G. O. Depaola, M. L. Iparraguirre, Nucl. Inst. Meth. A 611, 84 (2009).
7. D. Bernard, Nucl. Inst. Meth. A 729, 765 (2013).
8. D. C. Gates, R. W. Kenney and W. P. Swanson, Phys. Rev. 125, 1310 (1962).
9. E. L. Hart, G. Cocconi, V. T. Cocconi and J. M. Sellen. Phys. Rev. 115 678 (1959).
10. R. E. Ansoger, R. D. Baker, A. E. S. Krzesinski W .W. Neale, J. G. Rushbrooke and G. S. B. Street Phys. Rev. D 7, 26 (193).
11. J. A. Wheeler and W. E. Lamb, Phys. Rev. 55, 853 (1939).
12. L. Iparraguirre,G. O. Depaola, Eur. Phys. J. C 71, 1778 (2011).